Received 14 March 2024; revised 17 April 2024; accepted 5 May 2024. Date of publication 8 May 2024; date of current version 6 August 2024.

Digital Object Identifier 10.1109/OJAP.2024.3398147

RF Circuit Analysis of UWB Planar Log Periodic Antenna for 5G Communications Using Theory of Characteristic Modes

P. SUMITHRA[1] (Member, IEEE), MOHAMMED GULAM NABI ALSATH[2] (Senior Member, IEEE), K. J. JEGADISHKUMAR[3] (Member, IEEE), AND D. KANNADASSAN[4] (Senior Member, IEEE)

[1]Department of Engineering Design, Indian Institute of Technology Madras, Chennai 600036, India

[2]Department of Electrical and Communication Engineering, College of Engineering Guindy, Anna University, Chennai 600025, India

[3]Department of Electronics and Communication Engineering, Sri Sivasubramaniya Nadar College of Engineering, Chennai 603110, India

[4]School of Electronics Engineering, Vellore Institute of Technology, Vellore 632014, India

CORRESPONDING AUTHOR: D. KANNADASSAN (e-mail: dkannadassan@vit.ac.in)

This work was supported by the Science and Engineering Research Board (SERB), Government of India under Grant PDF/2022/001476.

ABSTRACT Fifth generation (5G) wireless communication systems demand compact and low-profile high gain wideband antenna. Planar log-periodic array antenna (pLPA) has such potential qualities for 5G base-station and user-devices. However, many important features and RF analysis are rarely elaborated for pLPA which include equivalent circuit modeling. In this article, authors present the systematic RF analysis, fabrication, and equivalent circuit modeling for sub-6GHz 5G application using theory of characteristic modes (TCM). The fabricated pLPA is designed to cover the 5G bands with a high gain of $>$ 5 dBi and a fractional bandwidth of $>$ 1. Using simulation tool based on method of moments, radiating and non-radiating modes are tracked and studied with detailed physics. These modes are modeled using analytically derived equivalent circuit and assembled in an RF/microwave circuit simulator. The characteristic mode analysis and RF circuit modeling of pLPA help in the advancement of future 5G RF front-end modules.

INDEX TERMS Planar log-periodic array antenna, 5G wireless systems, characteristic modes, equivalent circuit modeling.

I. INTRODUCTION

IN THE evolution of wireless communication systems, 5G/6G next generation technology standards targeted for low latency and high channel capacity. Also, they demand a large bandwidth and sub-3 dB noise figure [1]. Multiple antenna (MIMO) based phased-array systems are emerging to meet these demands which result high selectivity to achieve high SNR with required channel capacity. The New Radio (NR) technology of 5G suggest frequency bands of sub-10 GHz (410 - 7125 MHz) and millimeter wave (24.25 - 52.6 GHz) [1], [2]. Other high performance technologies, such as ultra-wideband (UWB), RF sensing and Internet-of-Things are participating in development of 5G/6G long term evaluation (LTE) platform [3], [4]. Therefore, the RF front-end (RF-FE) integration of transceiver modules, such as power amplifier, LNA, RF switches and MIMO antennas is needed under single substrate [5], [6]. To design successful RF-FE, a versatile electronic design and automation (EDA) simulation tool is required.

Among all RF-FE modules, antenna is the one of the sub-systems often designed using 3D EM simulation tool. However, it is difficult to analyze the performance of the RF-FE without an accurate antenna equivalent circuit model. Despite the fact that numerical simulations reliably predict antenna impedance and radiation patterns. But it is difficult to predict physics behind resonance and radiation processes in wideband antennas using numerical methods. However, equivalent circuit modeling (ECM) has ability to provide the physical insight of the resonance and useful in design of integrated matching circuits. Yet, it shall not provide detailed observations of radiation mechanism at various excitation frequencies. There are numerous equivalent circuit

schemes that were adopted to model impedance of antenna, like analytical model [7], series RLC networks, parallel RLC networks [8], [9], and singularity expansion method (SEM) [10]. Most of the ECM methods have been made to fit with reactive and radiating impedance of the antenna. But, for larger bandwidth, this fitting becomes highly inaccurate. Furthermore, the validity of these models for the present works on pLPA is not studied. It may be due to several reasons: 1) Unclear understanding of LPA's multiple resonances and anti-resonances, 2) large bandwidth, and 3) unclear radiation process from symmetric and asymmetric currents of LPA arms.

The theory of characteristic modes (TCM) has been employed to predict the behaviors of antennas. It features the great potentials in the analysis and physical understanding of the antennas with focus on radiation mechanism. Garbacz and Turpin [11] and Harrington and Mautz [12] are the pioneers of TCM for antenna design and optimization. Accurate equivalent circuit modeling of antenna can be developed with TCM. Interestingly, this approach was used in early stages of CMA by Yee and Garbacz in 1973 [13]. They have modeled both self-admittance and mutual admittance $Y_n(\omega)$ of delta-gaps in the wire as RLC elements. Along with CMA, EC modeling of center-fed dipole antennas is reported by Fabres [14]. Series RLC resonant circuit was proposed for each radiating modes of dipole. Alternatively, a high-pass RLC equivalent circuit model was proposed by Adams and Bernhard [15]. They have presented the wideband EC modeling of thin dipole antenna along with computed radiation patterns successfully. In our recent work, we have demonstrated the detailed modal analysis and EC modeling of wideband antennas using TCM [16]. The model helps in studying the mode-coupling and the formation of wideband. Also, the model extended to predict the radiation pattern of an antenna for any signaling frequencies within the desired spectrum.

Several wideband and ultra-wideband planar antennas, such as bowtie, spiral, log-periodic and Vivaldi antennas, were demonstrated with high gain in the last few decades. Amongst these, planar log-periodic antenna (pLPA) shows relatively uniform radiation characteristics over the large bandwidth. Also, pLPAs can operate more than 10:1 operational bandwidth with a gain $>$ 5 dBi. Yet, it is not a real frequency-independent antenna [17]. On the other hand, it shows self-complementary nature that rewards constant input impedance of approximately 188.5 Ohm (60π) which ease the antenna matching over a large bandwidth. In recent times, few reports on planar log-periodic antenna were demonstrated for 5G communications [18], [19]. However, no detailed reports on modern CMA or ECM of log-periodic antenna are found as per authors' knowledge. Here in this article, we elaborated the characteristic mode analysis and equivalent circuit model of wideband planar LPA antenna (pLPA) to predict resonance and radiation mechanism. Section II presents the CMA of pLPA in detail and characterizes the modal resonance over the desired wideband. From the understanding of modal analysis, the complete EC model is constructed with the help of modal equivalent circuit of radiating modes, presented in Section III. Finally, this model is further used to calculate the radiation patterns and gain over the large spectrum of pLPA.

II. CMA OF PLANAR LOG-PERIODIC DIPOLE ANTENNA

pLPA was proposed and developed long-back by DuHamel and Isbell [20]. Analytical and numerical modeling of LPAs were presented by many researchers. Wolter and Paul et al. had established the theory of LPA by solving the Maxwell's wave equation for wire and planar geometry [21], [22]. The theory yields the formulae for optimum high-directivity LPA for the given value of growth rate τ. This agrees with Carrel's approach [23]. Alternatively, Kazemipour et al. [24] reported the analytical modeling of the LPA antenna using shifted branches dipole antenna which was proposed by Evans [25]. It was found that the impedance and radiation characteristics of LPA are stable over the operating bandwidth. Although these analysis and predictions are useful, they are complex to accommodate the angular dipoles of pLPAs. Alternatively, Scheuring et al. presented an analytical model to compute the resonant frequencies of angular dipole LPA [17]. CMA of log-periodic wire dipole antenna was first performed by Hilbert and Balmain to understand the symmetric and asymmetric resonances [26]. It was observed that the structural asymmetry of LPA may cause side-lobe formation. In this section, the design and CMA of pLPA are presented in detail.

A planar self-complementary angular toothed pLPA was designed to cover the wide spectrum of 1 to 3 GHz. This frequency range covers the 5G NR bands [1]. From the calculation, this pLPA takes an outer diameter of $D_{out} = 2 \times R_{out} = 2 \times 72.4$ mm and inner diameter of $D_{in} = 2 \times 16.1$ mm. With the tooth and boom angles of $\alpha = \beta = 45°$ to achieve the self-complementary, a growth rate of τ =0.65 is adopted for the design. Fig. 1 (a) shows the layout of a planar LPA antenna with geometric parameters. Excitation and impedance matching of self-complementary pLPAs at the port are challenging as these structures show impedance of approximately 188.5 Ohm at the feeding apex point. Wideband balanced feeding baluns were proposed in early reports [27], [28], however they are complex in design and implementation. Hanumantha Rao et al., reported a simple planar tapered balun to feed self-complementary antennas which matches the unbalanced 50 ohms feed to 188 Ohms balanced line [29]. We adapted same planar tapered balun (PTB) which is presented in Fig. 1 (b) with dimensions. To feed the pLPA, this PTB was designed and optimized on the FR4 substrate with $\varepsilon_r = 4.4$ and $tan\delta = 0.0023$. The bottom ground plane of the microstrip PTB, measuring $L_{PTB} = 55$ mm, has a width of $W_G = 7$ mm. It tapers gradually to a parallel line width of $W_P = 0.534$ mm. The feed line, measuring $W_F = 1.53$ mm, is etched on top of the substrate to match 50 Ohms and smoothly tapers to W_P= 0.534 to balance 180 ohms. This structure along with integrated pLPA

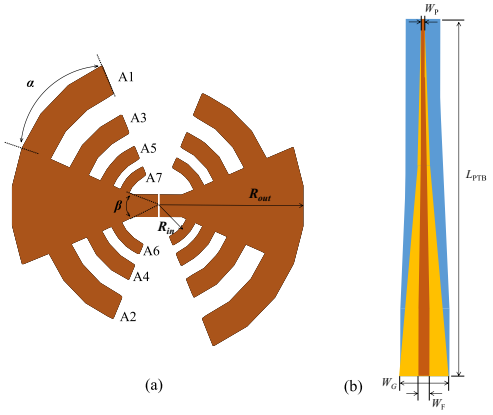

FIGURE 1. (a) Layout of Self-complementary toothed angular pLPA (b) Planar tapered balun.

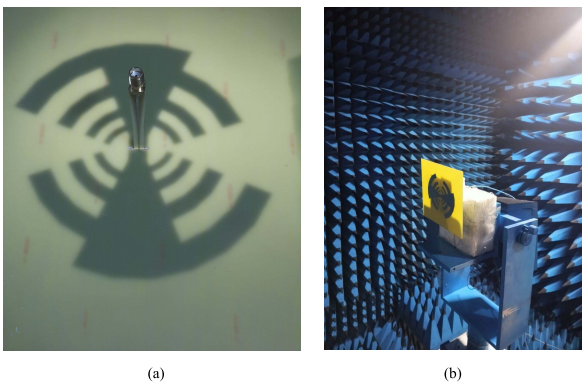

FIGURE 2. (a) Fabricated pLPA with integrated tapered balun. (b) Radiation pattern measurement setup in anechoic chamber.

was simulated using Ansys HFSS for full wave analysis to study the matching and radiation properties.

Both pLPA and PTB were fabricated using PCB mechanical etching tool with precision of 0.1 mm and integrated using micro-soldering process. Fig. 2 (a) shows the fabricated antenna with integrated PTB. The reflection-coefficient was measured using Agilent Technologies N9918A Field Fox microwave analyzer. Radiation patterns of fabricated antenna are measured, as shown in Fig. 2 (b), using the anechoic chamber with RF shielding of -110 dB. Fig. 3 (a) shows the simulated and measured reflection-coefficient and frequency dependent gain characteristics of proposed pLPA. It is evident that both simulation and measurement show good impedance matching for the desired bandwidth of 1 to 3 GHz. Yet, there are visible difference between the resonant frequencies of simulation and measurement. This shall be due the feeding PTB and integration tolerances. Minor inaccuracies in the calibration are also contributing factor for the variations in the measurement results. Further, the soldering of SMA to the PCB panel has contributed to additional losses which is not accounted in the simulation. Realized gain of pLPA of the frequency from simulation and measurement show that the antenna has uniform gain of ~ 5 dBi within the desired spectrum. Measured radiation patterns at various frequencies within the desired spectrum are presented in Fig. 3 (b-d) for principal planes $\phi = 0^o$ and $\phi = 90^o$. As expected, the dipole antenna radiation pattern with peak-gain of 5 dBi was observed. While dipole antennas show gain of ~ 2.14 dBi at resonance, the pLPA results 3 dBi higher which is explained with the help of modal analysis in the following sections. One shall observe that the pLPA has highly directional radiation pattern from the results along $\phi = 0^o$ and $\phi = 90^o$. The antenna exhibits broadside radiation perpendicular array axis with no visible sidelobes.

Later, the structure pLPA was simulated using Altair FEKO for modal analysis. Dominant 9 modes of pLPA are computed using MoM simulation with 128 RWG edge elements. Other higher order modes are ignored which are out of band and do not contribute for the resonance. Fig. 4 presents the computed eigenvalues of dominant 9 modes for pLPA antenna. On close observation, odd modes show the similar behavior of radiating modes of planar dipole antenna [16]. An odd mode exhibits highly capacitive ($\Lambda_n < 0$) at low frequencies and experiences resonance at f_{0n} ($\Lambda_n = 0$). After the resonance, the mode turns to be slightly inductive ($\Lambda_n > 0$) and slowly decreasing toward $\Lambda_n = 0$). However, at higher frequencies, next odd mode becomes dominant. To keep the orthogonality within the scope of computation, these odd modes exhibit the eigenvalue crossing avoidance (ECA) between themselves at $|\Lambda_n| > 1$ regions [30]. Yet, few odd modes (Mode-5 and Mode-7) show eigenvalue crossing which shall be due to numerical inconsistency in the modal tracking. Alternatively, the eigenvalues of even modes are rapidly growing from a high negative (capacitive) to a positive (inductive) value and crossing the odd modes. Between even modes, we can observe the ECA. These set of odd modes or even modes do not cross among themselves as they are eigentraces of same irreducible representation, thus they experience ECA. Due to the close occurrence of many resonances in pLPA and effect of ECAs, the coupling between modes is ignored.

Odd and even modes show dissimilar modal current patterns which are presented in Fig. 5 (a) and (b) respectively. Along with them, the modal far-field radiation patterns at the resonant frequencies of both eigenvectors are presented. The odd modes show modal currents maxima at center of the each tooth. Also, odd mode eigenvectors show symmetry between two respective teeth of opposite arms with respect to center of the antenna. Due to the symmetry, the effective modal current of odd modes is non-zero at feed position of dipole. This is similar to the resonance characteristic of planar dipole antenna which shows broadside radiation at natural resonance, as shown in Fig. 3 (b). It is worth to mention that there are two dipoles (arm A2 and A3) involved in radiation for a single odd mode and yields ~ 5 dBi. In the next odd mode, the arms A3 and A4 will participate in resonance and radiation. Due to this phenomenon, a uniform gain is maintained over the desired wide spectrum. From this understanding, one shall understand that the mode-1

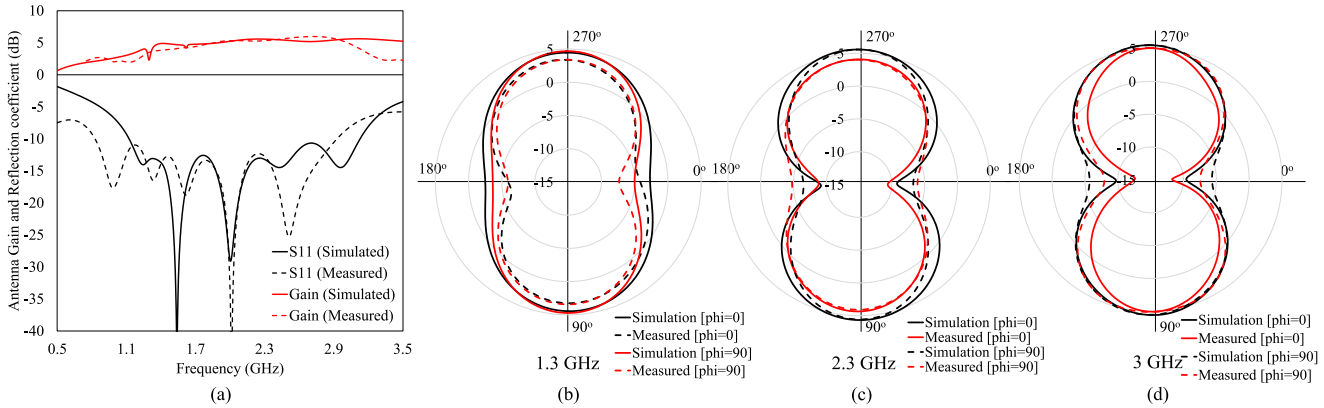

FIGURE 3. (a) Simulated and measured reflection coefficient and gain characteristics of proposed pLPA with integrated balun. (b-d) Simulated and measured radiation pattern at various frequencies for $\phi = 0^o$ and $\phi = 90^o$.

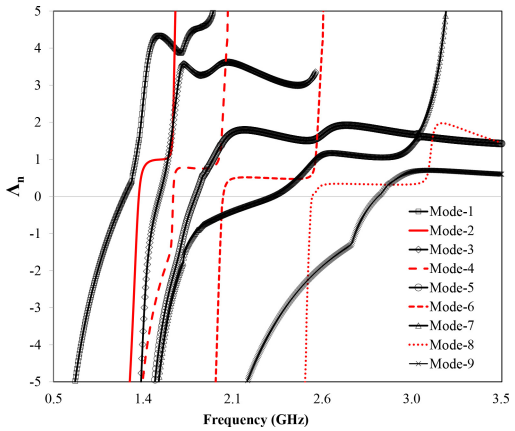

FIGURE 4. Computed eigenvalue of dominant odd and even modes within 0.5 to 3.5 GHz.

take dominant modal current at outer arm (A1) which is longer and wider. On the other hand, the modal resonances of mode-9 should be due to modal currents at inner short arms (A6 and A7). This is evident in Fig. 5 (d).

Modal significance (MS_n) presents the normalized amplitude of the modal currents, computed as $MS_n = |1 + j\Lambda_n|^{-1}$. Therefore, it is largely depending on the electrical behavior of the current modes according to the shape of the antenna. Fig. 6 (a) shows the MS_n of all current modes. One shall observe that the radiation bandwidth, corresponding to $MS_n = 0.707$, is increasing for higher radiating modes. It may be due to the involvement of multiple arms/teeth of pLPA for the higher current modes. In Fig. 5 (d), one shall observe that the mode-9 which has dominant current in three arms. Alternatively, the characteristic angle ($\delta_n = 180^o - tan^{-1}(\Lambda_n)$) computes the phase angle between a modal current (J_n) and modal far field (E_n). Therefore, one shall expect $\delta_n = 180^o$ around resonance and slope of δ_n determines the radiation bandwidth. Fig. 6 (b) presents the computed δ_n over the frequency. Unlike odd radiating modes, the non-radiating modes show fast transition from 270^o to 90^o. This indicates that non-radiating modes stores E and H near-fields over the desired bandwidth. However, these stored energies should be significantly low as the net modal currents, with respect to excitation point, is close to zero.

The modeling of multiple resonances in pLPA was reported to understand the origin of radiation and resonance mechanisms by few researchers. Often the resonant lengths of arms were modeled as $\lambda_g/2$ or $\lambda_g/4$ for the guided wavelength $\lambda_g = \lambda_0/\sqrt{\varepsilon_{eff}}$ [20]. With detailed analytical modeling, Scheuring et al. reported the resonance is originated in the anti-tooth of the pLPA, compared with $\lambda_g/2$ slot resonator [17]. It was observed from the full-wave simulation that the current maxima appears on anti-tooth of pLPA, flowing through bow-tie structure. In our observations in modal current and full-wave simulations without the substrate, the modal current are maxima at tooth and supports the $\lambda_g/4$ resonator model. On the other hand, the even modes exhibit currents traveling in opposite directions, can be seen in 5 (b). These currents in opposite arms cancel each other and results zero effective modal current for asymmetric even modes. Therefore, the even modes cannot be excited and do not contribute any radiation. However, the asymmetry/opposite currents on shifted dipole arms from the center radiate a weakly, perpendicular to main lobe of odd modes. These weak radiations form the side-lobes of pLPA. Similar observations on side-lobes of LPAs were reported in earlier studies [26].

III. EC MODELING OF PLANAR LOG-PERIODIC DIPOLE ARRAY ANTENNA

The equivalent circuit model of pLPA can be achieved by expressing the eigenvalue as function of circuit elements. Modal impedance of n^{th} characteristic mode is,

$$Z_n(\omega) = \frac{1}{J_n^2(\omega)}(1 + j\Lambda_n(\omega)) \quad (1)$$

Here, Λ_n and J_n are the eigenvalue and modal current of n^{th} characteristic mode. We have adopted 3^{rd} order equivalent circuit (3EC) of a series capacitor (C_n) with parallel RL section (R_n and L_n), shown in Fig. 7 (a), similar to our earlier work [16]. From the detailed analytical modeling of modal

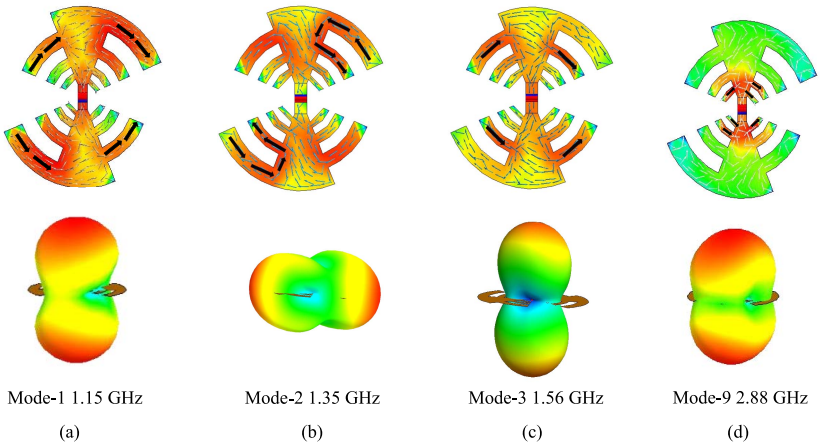

FIGURE 5. Modal current and far-field patterns of few odd and even modes (a) Mode-1, (b) Mode-2, (c) Mode-3, and (d) Mode-9.

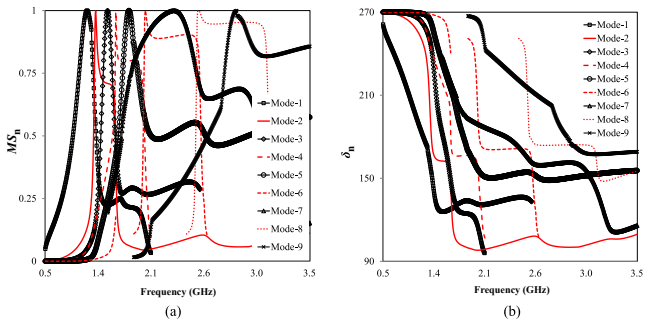

FIGURE 6. (a) Modal significance (MS_n) and (b) Characteristic angle (δ_n) of all dominant odd and even modes.

impedance [16], the equations of Λ_n and J_n^2 are obtained for high pass 3EC model as follows:

$$\Lambda_n = \frac{\omega^2(b_1 - a_1) - a_0 b_1}{\omega^3}; J_n^2 = \frac{\omega^2 + b_1^2}{\omega^2} \tag{2}$$

where, $a_1 = {}^1/_{R_n C_n}$, $a_0 = {}^1/_{L_n C_n}$, $b_1 = {}^{R_n}/_{L_n}$. The R_n, L_n and C_n can be computed using,

$$R_n = R_{0n}.R_{rn}; L_n = \frac{R}{\sqrt{Q_n}.\omega_{0n}}; C_n = \frac{1}{L.\omega_{0n}} \tag{3}$$

where, $\omega_{0n} = 2\pi f_{0n}$ and Q_n are angular frequency and modal quality factor at resonant frequency (f_{0n}) of n^{th} mode. The resistance, defined with normalized modal resistance R_{0n} and radiation resistance R_{rn}, can be computed using $R_n = \frac{R_{rn}}{J_n^2(f_{0n})}$. For dipole antenna, the typical value to $R_{rn} =$ 72 Ω. From Eq. (2), we get $J_n^2(f_{0n}) = \frac{\omega_{0n}^2 + b_1^2}{\omega_{0n}^2}$, where $b_1 = \frac{R}{L} = Q_n.\omega_{0n}$. The overall equivalent circuit model may be generated by parallelly cascading the 3EC models of the first two odd modes, mode-1 and mode-3. The anti-resonance in this case is created by the interaction of mode-1 and mode-3 modal reactances. Thus, a parallel resonant element, such as capacitor or inductor as shown in Fig. 7 (a), can be used to restore the imaginary part of admittance to zero. This shunt element reactance can be calculated by:

$$-X_{mn}(\omega') = Im(Y_m) + Im(Y_n) \tag{4}$$

The information about anti-resonance frequency ω' is acquired from results of measurement or full-wave simulation. Alternatively, one can add few higher order modes to achieve accurate wideband circuit of antenna which do not require parallel resonant element.

Considering severe ECA effects for pLPA, the development of equivalent circuit is a complicated work. Also, the computation of modal quality factor and modal current densities may not be reliable due to the same. To achieve the single solution of equivalent circuit for 9 modes over a large bandwidth, few compromises are taken. For simplicity, the 3EC model is accounted for all dipole modes of pLPA, similar to earlier cases. For each dipole mode, the values of R, L, C elements of 3EC model are calculated based on the best fitting with eigenvalues of MoM analysis by assuming optimum quality factor. Out of many possible combinations, two cases are presented here. Case-1 is the 3EC model for all dipole modes with high quality factor. On contrary, the case-2 accounts low quality factors for all modal 3ECs. Table 1 lists the resonant frequencies, Q factors and radiation resistance of 5 dipole modes for the case-1 and case-2. Compatibility between the eigenvalues of MoM simulation and equivalent 3EC models is presented for case-1 and case-2 in Fig. 7 (c) and (d) respectively. In both cases, a good fitting is observed, at least near the resonant frequencies. As expected, the variation between the eigenvalue of numerical simulation (MOM) and proposed model is visible at higher order modes. Unlike simple antennas, UWB log-periodic antenna has multiple modes, including non-radiating modes. This results severe ECA and visible difference between numerical simulation (MOM) and proposed model. However the eigenvalues of EC models are crossing, as the EC model of each mode is similar to auxiliary modes presented in [30]. Difference between case-1

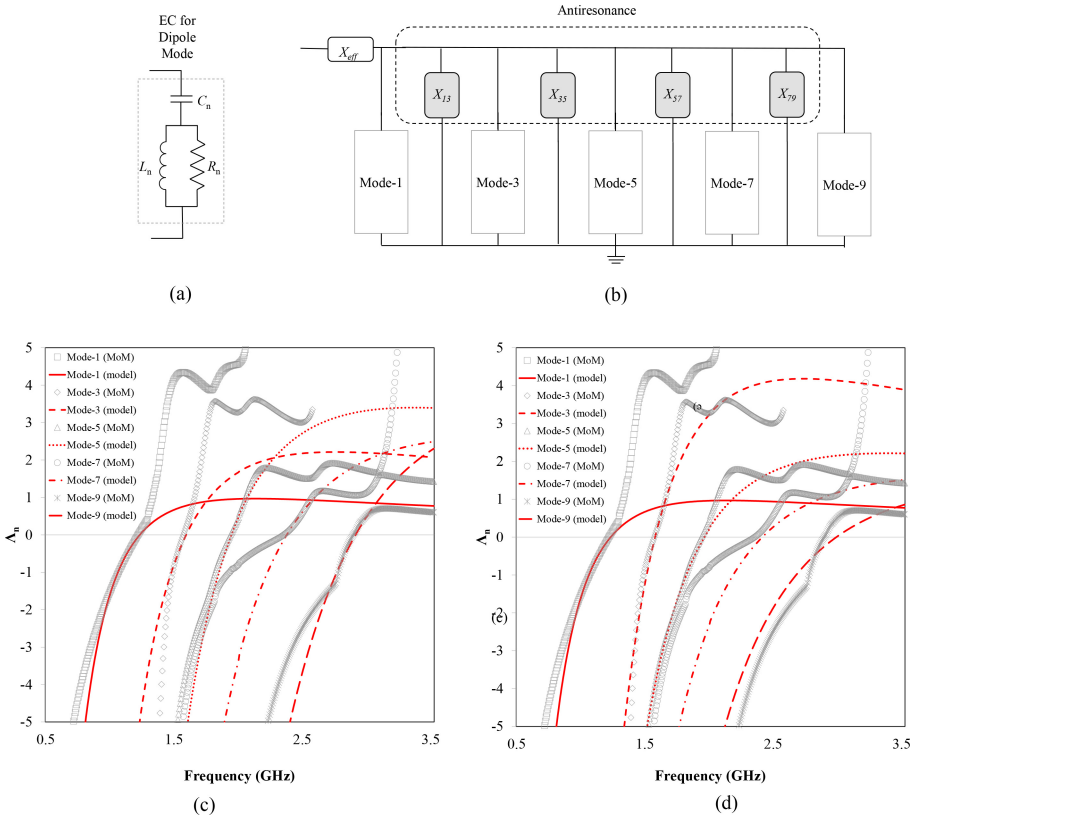

FIGURE 7. (a) Equivalence circuit (EC) model of pLPA with modal EC and parallel resonant elements, Eigenvalues of 3EC models with MoM data for (b) Case-1 and (c) Case-2.

and case-2 can be found in higher modes where eigenvalue maxima Λ_{max} show distinct difference due to difference in quality factors.

To achieve the over-all equivalent circuit, the shunt inductances/capacitances (L_{mn}/C_{mn}) are calculated using equ. 4 from the reactance of dipole modes at anti-resonance frequencies. This part is challenging as the reactance of 5 odd modes should be canceled with LC networks. So, we implemented in two phases as shown in Fig. 8, namely: 1) primary LC element and 2) secondary LC element, with following procedure. In the phase-1, at first, the reactance of mode-1 ($Im(Y_1)$) and mode-3 ($Im(Y_1)$) are calculated and computed $-X_{13}$ at anti-resonance of f'_{13}=1.43 GHz using Eq. (4). By placing a parallel L_{01} element, the effective reactance is canceled, which is shown as 'stage-1'. Then, the second anti-resonance at f'_{35} achieved by placing by L_{02} which is calculated with total reactance due to effective reactance $X_{13,eff} = Im(Y_{stage-1})$ of stage-1 and reactance of mode-5 ($Im(Y_5)$). Similarly, third and fourth anti-resonances at 2.04 GHz and 2.51 GHz were achieved using L_{03} and L_{04}, respectively. Again, the over-all reactance is canceled at all anti-resonances with secondary LC elements (phase-2), L_{11}, L_{22}, L_{33} and L_{44}. The L_{0n} or L_{mn} can be inductor or capacitor based on the reactance to be canceled. This procedure successfully yields the over-all equivalent circuit for both case-1 and case-2. All R, L, C elements are listed in Table 1.

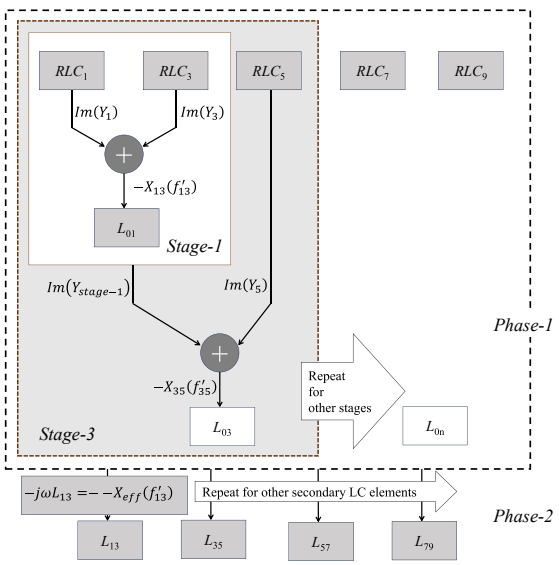

FIGURE 8. Implementation flow diagram of over-all equivalent circuit of UWB pLPA for case-1 and case-2.

The reflection coefficients calculated from full wave simulation is compared with circuit simulation of EC for case-1 and case-2 in Fig. 9 (a). In both cases, the bandwidth coverage is properly achieved. As the case-1 took higher Q

TABLE 1. Calculated EC model parameters for dipole modes of pLPA antenna for case-1 and case-2.

Mode	f_{0n}(GHz)	$R_{rn}(\Omega)$	Case-1						
			Q_n	$R_n(\Omega)$	$L_n(nH)$	$C(pF)$	f'_{0n} (GHz)	C_{0n}/L_{0n}	C_{mm}/L_{mm}
1	1.15	166.14	3	720	33.04	0.57	1.36	297.82 nH	165.60 nH
3	1.56	214.99	11	8784	81.37	0.13	1.74	0.23 pF	18.39 nH
5	1.92	194.16	9	5904	54.32	0.13	2.13	506.94 nH	0.07 pF
7	2.34	178.31	7	3600	34.95	0.13	2.61	0.09 pF	0.16 pF
9	2.88	182.81	9	5904	36.27	0.08			

Mode	f_{0n}(GHz)	$R_{rn}(\Omega)$	Case-2						
			Q_n	$R_n(\Omega)$	$L_n(nH)$	$C(pF)$	f'_{0n} (GHz)	C_{0n}/L_{0n}	C_{mn}/L_{mn}
1	1.15	166.14	3	597	30.44	0.62	1.36	35.36 nH	13.09 nH
3	1.56	214.99	6	2664	45.24	0.23	1.74	0.37 pF	0.05 pF
5	1.92	194.16	6	2664	36.77	0.19	2.13	0.03 pF	0.10 pF
7	2.34	178.31	5	1530	23.11	0.20	2.61	60.00 nH	0.13 pF
9	2.88	182.81	4	1224	16.92	0.18			

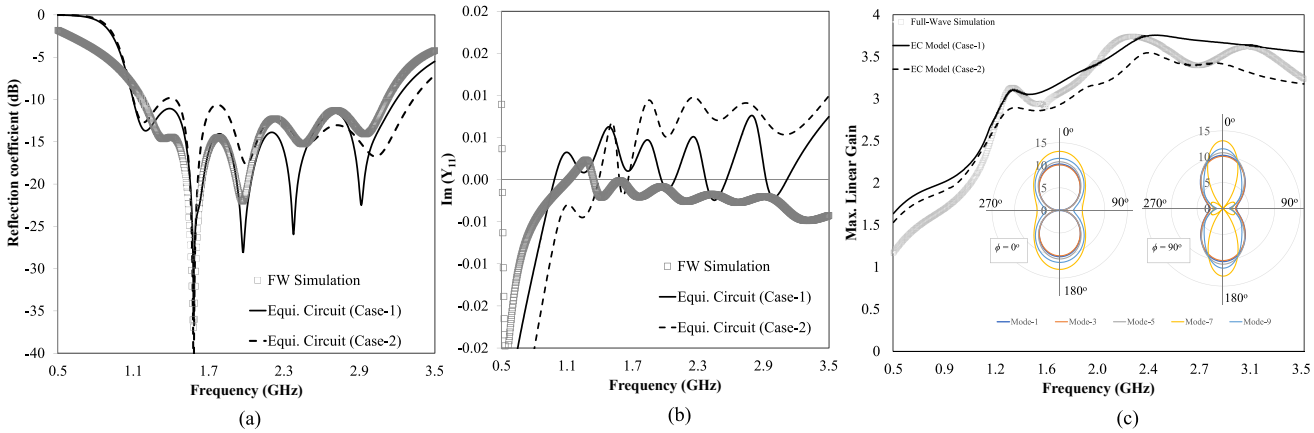

FIGURE 9. (a) Compatibility of S_{11} of ECs for case-1 and case-2 with full wave simulation. Computed (b) real-imaginary admittance and (c) maximum linear gain from EC models and FW simulation. (inset) Modal fields of five dipole modes at f_{0n} for $\phi = 0^o$ and $\phi = 90^o$.

values, it exhibits a multi-resonance response which shows excellent match with full wave simulation. On the other hand, case-2 shows a moderate fit in the lower band of spectrum while the fitting is not proper in higher band. Due to the large bandwidth of each mode for lower Q influences the other mode which may result a poor fitting. To quantify the fitting, the imaginary part of admittances from full wave and circuit simulations are compared, the compatibility is presented in Fig. 9 (b). Due to high quality factor, the case-1 EC exhibits multiple zero crossing clearly at anti-resonance frequencies. However, the EC of case-2 shows similar oscillation and rarely crosses zero. This is due to the overlapping of modal reactance of multiple modes.

Computation of far-field radiation patterns at any frequency within the desired spectrum can be performed using EC circuit. This was first demonstrated by Adams and Bernhard [15]. For an antenna, the total far-field is calculated by superposition of modes associated excited characteristic fields, that is:

$$E_T(\theta, \phi) = \sum \frac{J_n(m)}{(1 + j\Lambda_n)} E_n(\theta, \phi) \tag{5}$$

where Eigenvalue Λ_n and eigenvector J_n are obtained from eqns. (2). The E_n is calculated from MoM simulation at natural resonances, corresponding to $\Lambda_n = 0$ of n^{th} mode. Inset of Fig. 9 (c) shows the modal radiation patterns of all dipole modes at their frequency of resonance. The characteristic modal fields associated with the dipole modes exhibit similar radiation patterns. However, the major lobe becomes narrow for modes at high frequencies. Along with these modal fields E_n, Λ_n and J_n of EC model of each dipole modes are used to calculate the total characteristic far field at the entire frequencies of the spectrum. Fig. 9 (c) presents the calculated linear gain from EC models of both cases and FW simulation. Both case-1 and case-2 EC models predict the antenna gain with acceptable accuracy. As case-1 takes high Q for EC modeling, the weights of modal fields change drastically over the bandwidth. This results high gain and high ripple magnitude (~ 1.2) within the desired bandwidth. In case-2, the low Q factor for modes increases the modal bandwidth and results slow variation in modal weights. This yields low gain over the spectrum compared to FW simulation result. Optimum choice of Q and accurate modeling of characteristic modes shall predict

TABLE 2. A comparison of RF circuit models for the wideband antennas.

Reference	Theory	EC model	Antenna	Elements	Frequency	Compatibility	Complexity
[31]	FCF	Hybrid RLC	ESA	> 5	1 to 5	Moderate	Complex
[32]	CCE	Hybrid RLC	Chassis	4	05 to 2.5	Moderate	Complex
[33]	OEM	Hybrid RLC	ESA	3	0.1 to 0.4	Moderate	Complex
[34]	TCM	parallel RLC	dipole	3	0.1 to 0.3	Moderate	Easy
[14]	TCM	series RLC	dipole	3	0.2 to 0.4	Moderate	Easy
[15]	TCM	High-pass RLC	dipole	3	0.1 to 1	Excellent	Moderate
This work	TCM	High-pass RLC	pLPA	3	1 to 3	Excellent	Moderate

the radiated fields and gain accurately. The EC modeling of pLPA reveals that the uniform gain over such a large bandwidth is mainly due to dipole or symmetric modes whose resonant frequencies are close to each other. This supports the theory of resonance phenomena proposed by Hilbert and Balmain [26].

A comprehensive summary of various RF circuit modeling approaches of wideband antennas is presented in Table 2. A detailed circuit analysis using Foster canonical forms (FCF) for UWB electrically small antenna (ESA) was reported by Wang et al. [31]. Althrough, the hybrid RLC elements show good compatibility for UWB pulses analysis, the multiple RLC elements of the model make the computational complexity. Jari Holopainen et al., reported the EC topology with coupled capacitive element (CCE) to model the EM coupled chassis antenna in mobile handset [32]. The work results good matching and ease of integration with large antenna, yet the theory is not tested in other compatible antennas. Using odd and even mode (OEM) analysis, EC model was developed for two-segmented capped monopole antenna by Stuart [33]. Although this model exhibits moderate compatibility with the antenna impedance, the circuit model is complex and not tested beyond ESAs. TCM inspired EC modeling for dipole antenna was successfully reported by Fabres [14] and Adams and Bernhard [15]. The series RLC modeling approach is straightforward and covers a narrow bandwidth of 0.2 GHz with simple and easy computation. Alternatively, the model developed by Adams et al., showed an excellent accuracy on modeling the eigenvalues or impedance function of dipole antennas. However, the modeling is not a direct and easy method. Khaled Obeidat et al., presented the parallel RLC circuit for center-fed dipole and patch antennas [34]. The proposed model can give moderate compatibility with the impedance function of MOM data of these antennas. In comparison to these important reports, the proposed modeling approach for wideband and UWB antennas stands with excellent compatibility with moderately complex implementation. With cascading approach, the impedance and antenna gain of pLPA with large bandwidth were predicted by TCM inspired 3EC model. Considering the forementioned facts, one shall work on equivalent circuit modeling for MIMO, fractal, ultra-wideband, multi-mode and array antennas. Low-profile slot antennas are often considered for several consumer electronic applications [35], yet equivalent circuit model of such antennas are rarely reported. Using electric and magnetic CMs, one shall model the multiple resonances in slot or chassis antennas for better impedance matching. The calculation of radiated fields shall account frequency dependent and polarization dependent factors in the equation of the total modal radiated fields. This approach may yield accurate calculations for gain of wideband ultra-wideband antennas. The Equivalent circuit modeling can also be used to handle link budget, power budget analysis and antenna placement issues in various wireless applications, in particular 5G RF-FEs.

IV. CONCLUSION

We provided a comprehensive characteristic mode analysis and equivalent circuit modeling of planar angular LPA antenna in this work. The modal analysis of pLPA reveals the origin of resonance mechanism by decomposing the several characteristic modes. It is observed that two dipole arms are simultaneously excited at modal resonance and responsible for the radiation mechanism of LPA. Using analytical modeling, pLPA is modeled using 3^{rd} order equivalent RLC circuit which shows excellent compatibility with FW simulation. Although the eigenvalue crossing avoidances between odd modes are severe, the modeling procedure gives optimum equivalent circuit. The prediction of far field radiation patterns over a large spectrum was demonstrated with EC models. It was observed that the multiple modes are participating in the formation uniform antenna gain over the bandwidth. The proposed EC model is accurate enough that it may be utilized in the SPICE simulator to examine the link budget and power budget of the transmitter and receiver RF front-ends without the need for three-dimensional EM solvers.

ACKNOWLEDGEMENT

The authors thank Altair Engineering for supporting them with research license of FEKO. Authors thank Sudarshan B S and Pulipaka Srikantha for the process involved in soldering and antenna fabrication.

REFERENCES

[1] A. Gupta and R. K. Jha, "A survey of 5G network: Architecture and emerging technologies," *IEEE Access*, vol. 3, pp. 1206–1232, 2015.
[2] M. Hirzallah, M. Krunz, B. Kecicioglu, and B. Hamzeh, "5G new radio unlicensed: Challenges and evaluation," *IEEE Trans. Cogn. Commun. Netw.*, vol. 7, no. 3, pp. 689–701, Sep. 2021.

[3] S. Wijethilaka and M. Liyanage, "Survey on network slicing for Internet of Things realization in 5G networks," *IEEE Commun. Surveys Tuts.*, vol. 23, no. 2, pp. 957–994, 2nd Quart., 2021.
[4] A. Al-Fuqaha, M. Guizani, M. Mohammadi, M. Aledhari, and M. Ayyash, "Internet of Things: A survey on enabling technologies, protocols, and applications," *IEEE Commun. Surveys Tuts.*, vol. 17, no. 4, pp. 2347–2376, 4th Quart., 2015.
[5] F. Balteanu, "Circuits for 5G RF front-end modules," *Int. J. Microw. Wireless Technol.*, vol. 15, no. 6, pp. 909–924, 2023.
[6] T.-K. Le, U. Salim, and F. Kaltenberger, "An overview of physical layer design for ultra-reliable low-latency communications in 3GPP releases 15, 16, and 17," *IEEE Access*, vol. 9, pp. 433–444, 2021.
[7] R. Collin, *Antennas and Radiowave Propagation* (Electrical and Computer Engineering). New York, NY, USA: McGraw-Hill, 1985.
[8] M. Hamid and R. Hamid, "Equivalent circuit of dipole antenna of arbitrary length," *IEEE Trans. Antennas Propag.*, vol. 45, no. 11, pp. 1695–1696, Nov. 1997.
[9] B. Long, P. Werner, and D. Werner, "A simple broadband dipole equivalent circuit model," in *Proc. IEEE Antennas Propag. Soc. Int. Symp.*, 2000, pp. 1046–1049.
[10] G. Streable and L. Pearson, "A numerical study on realizable broadband and equivalent admittances for dipole and loop antennas," *IEEE Trans. Antennas Propag.*, vol. 29, no. 5, pp. 707–717, Sep. 1981.
[11] R. Garbacz and R. Turpin, "A generalized expansion for radiated and scattered fields," *IEEE Trans. Antennas Propag.*, vol. 19, no. 3, pp. 348–358, May 1971.
[12] R. Harrington and J. Mautz, "Theory of characteristic modes for conducting bodies," *IEEE Trans. Antennas Propag.*, vol. 19, no. 5, pp. 622–628, Sep. 1971.
[13] A. Yee and R. Garbacz, "Self-and mutual-admittances of wire antennas in terms of characteristic modes," *IEEE Trans. Antennas Propag.*, vol. 21, no. 6, pp. 868–871, Nov. 1973.
[14] M. C. Fabres, "Systematic design of antennas using the theory of characteristic modes," Ph.D. dissertation, Dept. Antennas Propag. Lab., Valencia Polytechn. Univ., Valencia, Spain, 2007.
[15] J. J. Adams and J. T. Bernhard, "Broadband equivalent circuit models for antenna impedances and fields using characteristic modes," *IEEE Trans. Antennas Propag.*, vol. 61, no. 8, pp. 3985–3994, Aug. 2013.
[16] P. Sumithra and D. Kannadassan, "Design and modeling of wideband planar antennas using characteristics modes," *IEEE Trans. Antennas Propag.*, vol. 69, no. 12, pp. 8257–8270, Dec. 2021.
[17] A. Scheuring, S. Wuensch, and M. Siegel, "A novel analytical model of resonance effects of log-periodic planar antennas," *IEEE Trans. Antennas Propag.*, vol. 57, no. 11, pp. 3482–3488, Nov 2009.
[18] Q.-X. Chu, X.-R. Li, and M. Ye, "High-gain printed log-periodic dipole array antenna with parasitic cell for 5G communication," *IEEE Trans. Antennas Propag.*, vol. 65, no. 12, pp. 6338–6344, Dec. 2017.
[19] I. M. M. Ibrahim, M. I. I. Ahmed, H. M. M. Abdelkader, and M. M. Elsherbini, "A novel compact high gain wide-band log periodic dipole array antenna for wireless communication systems," *J. Infrared Mil. Terahertz Waves*, vol. 43, pp. 872–894, Dec. 2022.
[20] R. DuHamel and D. Isbell, "Broadband logarithmically periodic antenna structures," in *Proc. IRE Int. Conv. Record*, 1957, pp. 119–128.
[21] J. Wolter, "Solution of maxwell's equations for log-periodic dipole antennas," *IEEE Trans. Antennas Propag.*, vol. 18, no. 6, pp. 734–741, Nov. 1970.
[22] A. Paul and I. Gupta, "An analysis of log periodic antenna with printed dipoles," *IEEE Trans. Microw. Theory Techn.*, vol. 29, no. 2, pp. 114–117, Feb. 1981.
[23] R. Carrel, "The design of log-periodic dipole antennas," in *Proc. IRE Int. Conv. Record*, 1961, pp. 61–75.
[24] A. Kazemipour, H. Kokabi, and A. Gaugue, "Modeling of a shifted branches dipole antenna, application to a log periodic antenna," *Electromagnetics*, vol. 23, no. 4, pp. 361–371, 2003.
[25] B. G. Evans, "Potential integral theory for a log-periodic dipole array of n, parallel, non-staggered," *Radio Electron. Eng.*, vol. 39, no. 4, pp. 224–232, 1970.
[26] M. Hilbert and K. Balmain, "Characteristic-mode analysis of symmetric and asymmetric log-periodic dipole antennas," in *Proc. Antennas Propag. Soc. Int. Symp.*, 1985, pp. 199–202.
[27] R. Jacques and D. Meignant, "Novel wide band microstrip balun," in *Proc. 11th Eur. Microw. Conf.*, 1981, pp. 839–843.
[28] Z.-Y. Zhang, Y.-X. Guo, L. C. Ong, and M. Y. W. Chia, "A new wideband planar balun on a single-layer PCB," *IEEE Microw. Wireless Compon. Lett.*, vol. 15, no. 6, pp. 416–418, Jun. 2005.
[29] P. H. Rao, M. Sreenivasan, and L. Naragani, "Dual band planar spiral feed backed by a stepped ground plane cavity for satellite boresight reference antenna applications," *IEEE Trans. Antennas Propag.*, vol. 57, no. 12, pp. 3752–3756, Dec. 2009.
[30] K. R. Schab, J. M. Outwater, M. W. Young, and J. T. Bernhard, "Eigenvalue crossing avoidance in characteristic modes," *IEEE Trans. Antennas Propag.*, vol. 64, no. 7, pp. 2617–2627, Jul. 2016.
[31] S. B. T. Wang, A. M. Niknejad, and R. W. Brodersen, "Circuit modeling methodology for UWB omnidirectional small antennas," *IEEE J. Sel. Areas Commun.*, vol. 24, no. 4, pp. 871–877, Apr. 2006.
[32] J. Holopainen, R. Valkonen, O. Kivekas, J. Ilvonen, and P. Vainikainen, "Broadband equivalent circuit model for capacitive coupling element–based mobile terminal antenna," *IEEE Antennas Wireless Propag. Lett.*, vol. 9, pp. 716–719, 2010.
[33] H. R. Stuart, "Eigenmode analysis of a two element segmented capped monopole antenna," *IEEE Trans. Antennas Propag.*, vol. 57, no. 10, pp. 2980–2988, Oct. 2009.
[34] K. A. Obeidat, B. D. Raines, and R. G. Rojas, "Discussion of series and parallel resonance phenomena in the input impedance of antennas," *Radio Sci.*, vol. 45, no. 6, pp. 1–9, Dec. 2010.
[35] P. Sumithra and D. Kannadassan, "Bandwidth enhancement of low-profile slot antennas using theory of characteristic modes," *AEU Int. J. Electron. Commun.*, vol. 138, Aug. 2021, Art. no. 153868.